A thesis submitted for the degree of
Bachelor of Science in Astronomy & Astrophysics

From the Fire: A Deeper Look at the Phoenix Stream

Kiyan Tavangar

The Department of Astronomy & Astrophysics
University of Chicago
Chicago, IL
May 2021

Advisor: Prof. Alex Drlica-Wagner
Graduation Date: June 12, 2021

Draft version May 14, 2021
Typeset using LaTeX **twocolumn** style in AASTeX63

From the Fire: A Deeper Look at the Phoenix Stream

ABSTRACT

We use six years of data from the Dark Energy Survey (DES) to present a detailed photometric characterization of the Phoenix stream, a thin, dynamically cold, low-metallicity stream in the southern hemisphere. We use natural splines, a non-parametric modelling technique, to simultaneously fit the stream track, width, and linear density. We recover four peaks and four gaps in linear intensity along with fluctuations in the stream track. We therefore conclude that Phoenix is a clumpy stream with linear intensity variations on degree scales, as well as wiggles in the stream track on $\approx$ 2-degree scales, signaling that the stream was likely disturbed during its formation and/or evolution. This improved stream model allows us to perform improved measurements of the distance (17.38 ± 0.08 kpc) and distance gradient (-0.01 ± 0.02 kpc/deg when using stream coordinates) of Phoenix. Such small-scale fluctuations are not common in other thin streams and the study of Phoenix offers a unique perspective on the ways that gravitational perturbations effect stellar streams. We discuss possible sources of perturbations to Phoenix including baryonic structures in the Galaxy, dark matter subhalos, or the influence of a parent satellite during the time of stream formation.

1. INTRODUCTION

Near-field cosmology utilizes observations of the smallest cosmological structures to answer fundamental questions about the composition and evolution of our universe. One of the major goals of near-field cosmology is to measure the distribution of dark matter in the local universe, which could lead to a better understanding of galaxy formation, structure, and evolution (Conroy & Wechsler 2009; Guo et al. 2013; Becker 2015; Wechsler & Tinker 2018). Recent advances in the discovery, measurement, and modeling of stellar streams around the Milky Way provide an exciting new avenue to advance the study of dark matter. Stellar streams are the tidally disrupted remnants of satellite galaxies and globular clusters. Their abundance and orbital histories enable tests of galaxy formation, accretion history, and stellar halo formation (e.g., Johnston 1998; Helmi & White 1999; Bonaca et al. 2019). Dynamically cold streams originating from disrupting star clusters are extremely sensitive to gravitational perturbations from massive substructures (e.g., Erkal & Belokurov 2015a; Bonaca et al. 2019). The study of stellar streams is thus a promising avenue for studying the distribution of dark matter at sub-galactic scales.

Large digital sky surveys have advanced rapidly since the Sloan Digital Sky Survey was used to discover tidal tails emanating from the Palomar 5 globular cluster (Odenkirchen et al. 2001; Rockosi et al. 2002; Odenkirchen et al. 2002, 2003). The known population of stellar streams has drastically expanded due to the development of data sets and techniques to probe the Milky Way halo at larger distances (Belokurov et al. 2006). Recently, increases in survey sensitivity have led to another rapid increase in the known population of stellar streams. In particular, deep imaging and precise photometry from the Dark Energy Survey (DES; DES Collaboration 2005, 2016) has yielded a large and diverse population of stellar streams in the southern hemisphere (Drlica-Wagner et al. 2015; Balbinot et al. 2016; Shipp et al. 2018).

Among the streams discovered by DES, the Phoenix stream is of particular interest due to its prominence, clumpy morphology, and low metallicity, as well as the fact that it is thin and kinematically cold. The stream was discovered in early data from DES by Balbinot et al. (2016). Broadly speaking, streams originating from globular clusters (such as Pal 5 or ATLAS) are thinner than those generated from dwarf galaxies (such as Sagittarius) (Grillmair & Carlin 2016). The narrow width of Phoenix ($\sim$ 0.14 deg) suggests that it likely originated from a disrupted globular cluster. Additionally, while globular cluster streams have an internal metallicity spread of zero, dwarf galaxy streams tend to have ones larger than $0.2 - 0.3$ dex. Wan et al. (2020) found $\sigma_{[\mathrm{Fe/H}]} \approx 0$ for Phoenix which strongly indicates it comes from a globular cluster. If Phoenix originated from a globular cluster, then it would be the most metal-poor globular cluster known, with a metallicity of [Fe/H] $= -2.7$. However, no clear progenitor system has been found.

A more detailed analysis of the spatial structure of Phoenix increases the relatively small number of cold

thin streams with similar modeling, which currently includes Palomar 5 (Erkal et al. 2017), Orphan (Koposov et al. 2019), ATLAS and Aliqa Uma (Li et al. 2020), and Jet (Ferguson et al. 2021). Combining density variation information from these streams can provide valuable information about the abundance of dark matter subhalos, which are predicted to be plentiful in conventional models of cold dark matter (CDM) (Diemand et al. 2005; Wang et al. 2020). Furthermore, we might be able to determine not only the way in which these subhalos disrupt baryonic structures such as streams but also potentially their location and density within the galaxy (e.g., Bonaca et al. 2019). A better measurement of stream uniformity can also give hints about the progenitor system (Malhan et al. 2020).

In this paper, we perform an improved analysis of the Phoenix stream using a photometric catalog derived from 6 years of DES imaging. We present detailed observational data and create a model of the stream to obtain better measurements of the stream track, width, intensity, and distance gradient. We also model the orbit of the stream in the Milky Way potential using member star radial velocities and proper motions from the Southern Stellar Stream Spectroscopic Survey (S^5 Li et al. 2019) and Gaia EDR3 (Gaia Collaboration et al. 2016; Brown et al. 2021), respectively.

The structure of this paper is as follows. In Section 2, we describe the DES and S^5 data sets used in this analysis. In Section 3, we describe our matched filter selection process to generate the best data to be used for the stream model. In Section 4, we present the stream model and discuss its results. We then apply those findings to give a new calculation of the distance gradient and use an orbit model to lend credence to our results. In Section 5, we discuss the density variations and stream track variations detected in the models and give possible explanations for each. Finally, in Section 6, we conclude.

2. DATA SET

DES is a six-year optical/near-infrared imaging survey covering $\sim 5000\,\mathrm{deg}^2$ of the southern Galactic cap in five visible/near-infrared filters, *grizY*, using the Dark Energy Camera (DECam; Flaugher et al. 2015) mounted at the prime focus of the 4-m Blanco telescope at the Cerro Tololo Inter-American Observatory (CTIO). The uniform and wide-area imaging over a large section of the southern sky allows deep searches for stellar streams as demonstrated by the numerous new stream discoveries using the DES Year 3 data (Shipp et al. 2018). In this paper, we use catalog data derived from the full six-year DES coadded images (Abbott et al. 2021). The deeper data provided by three additional years allows a more accurate characterization of stellar streams than has been done in the past.

The DES images were processed using the DES data management pipeline (Morganson et al. 2018). After photometric calibration using the Forward Global Calibration Method (FGCM, Burke et al. (2017)), the images were coadded to increase imaging depth. Our data set follows the same image-level processing and coaddition described in Abbott et al. (2021); however, it is augmented with value-added properties derived from multi-epoch fitting used for DES cosmology (e.g., Drlica-Wagner et al. 2018; Sevilla-Noarbe et al. 2020). We apply a morphological filter to select high-probability stellar sources by using an updated version of the `EXTENDED_CLASS` classifier used for the Y3 Gold release, described in Section 6.1 and Appendix B of Sevilla-Noarbe et al. (2020). The classifier for Y6 was adapted for updates to the SOF photometry of the deeper data. This is achieved in practice by taking `EXT_SOF<2`, choosing high confidence stars and candidate stars for our search.

3. METHODS AND ANALYSIS

To characterize the stellar population of the Phoenix stream, we further refine our object selection with a matched filter in color magnitude space. Using the technique described in Section 3.1 of Shipp et al. (2018), we select stars outlined by a synthetic isochrone from Dotter et al. (2008) and implemented in `ugali` (Bechtol et al. 2015; Drlica-Wagner et al. 2015).[1] We attempt to use the previously measured metallicity value for Phoenix of $Z = 0.00004$ as reported by Wan et al. (2020), but found that this is too metal-poor to be a part of the Dotter isochrone catalog. As a result, we are forced to use $Z = 0.00007$, the lowest metallicity value provided by the catalog. This 0.00003 difference does not make a significant difference along the main sequence, where the vast majority of our selected stars lie. We are therefore comfortable using this slightly different value to perform our search. For the age, we perform a 3-parameter MCMC search to find the age, distance modulus, and richness yielding the best fitting isochrone for the color-magnitude plots. This returns a value of 12.8 ± 0.2 Gyrs. For the distance modulus we use an iterative process involving the output of our model described in Section 4. We start by using the value found by the MCMC search described above of $m - M = 16.2$ and generate our results using this isochrone. With

[1] https://github.com/DarkEnergySurvey/ugali

those results, we are able to give a better measurement of the distance modulus and gradient as described in Section 4.2, giving us an updated value for which to rerun the matched filter selection and model. This iterative process eventually yielded a distance modulus value of 16.3, which we use for the final version of our matched filter analysis. These measurements allow us to perform an improved selection of Phoenix members relative to previous analyses of the stream in Balbinot et al. (2016) and Shipp et al. (2018). We also limit our selection to an absolute magnitude of $M_g < 3.4$ to ensure we choose stars along the main sequence, which has a higher signal-to-noise ratio. The final cut of stars in color-magnitude space is outlined in Fig. 1.

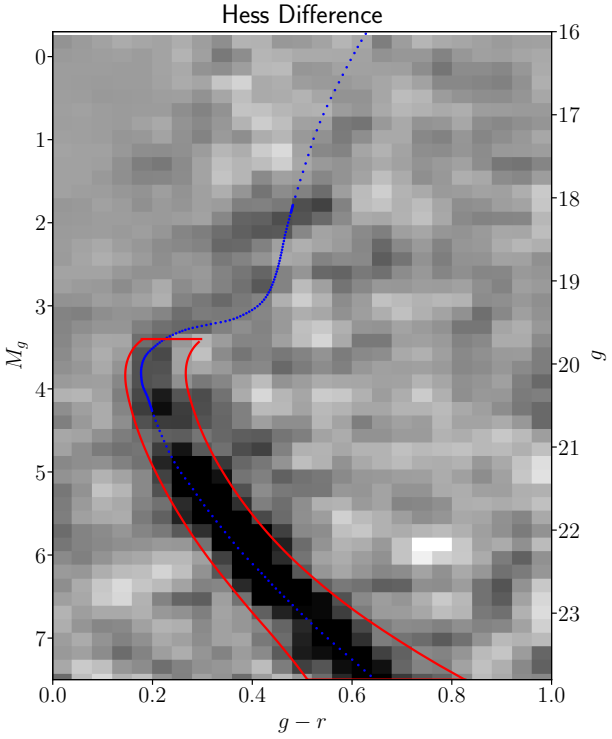

Figure 1. A Hess difference plot created by subtracting a background region above Phoenix (in Φ_2) of equal area to the stream. The main sequence is clearly visible. The Dotter et al. (2008) is shown in blue with parameters of $z = 0.00007$, $\tau = 12.8$ Gyr, and $m - M = 16.3$. This isochrone is selected as part of an iterative process where we take the output of the stream model described in Section 4 and find its distance gradient and average distance modulus, which informs an updated isochrone selection. The onstream region is selected in a similar iterative way using the stream track and stream width outputs of the model.

We then scan our isochrone filter across the range of distance moduli from $15 < m - M < 20$ in steps of size 0.1 mag. We fit a fifth-order background polynomial at each step and smooth the data using a Gaussian filter with a smoothing kernel of size $0.^{\circ}15$. From a visual inspection of the results, we confirm that the significance of the signal from the Phoenix stream is maximized at a distance modulus of $m - M = 16.3$ (shown in Fig. 2), in good agreement with the value reported by Balbinot et al. (2016).

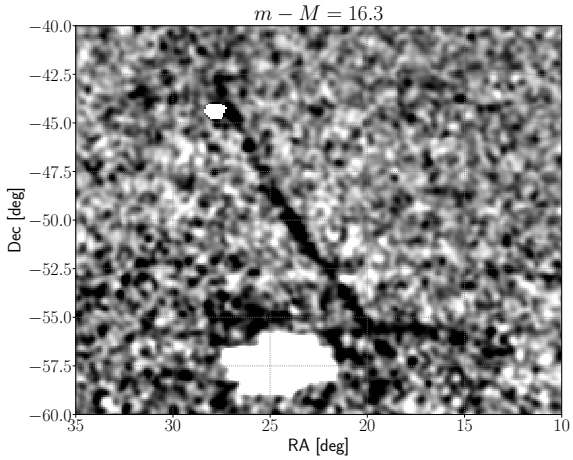

Figure 2. A spatial density map of the Phoenix stream and the region around it. The map is made using a matched filter selection represented by the red area outlined in Fig. 1 with isochrone parameters $z = 0.00007$, $\tau = 12.8$ Gyr, and $m - M = 16.3$. We note the horizontal feature to the southwest of the stream at Dec ≈ -55. This feature is not believed to be related to the Phoenix stream due to its very different track direction.

4. RESULTS

4.1. *Stream Track Model*

We build a model for the track, width, and intensity of the Phoenix stream. Our procedure is based off of similar models introduced in Erkal et al. (2017) and Koposov et al. (2019), and it is nearly identical in setup to that used in Li et al. (2020). We utilize the `STAN` programming language, which is specialized for statistical modeling and provides an easy interface to specify probabilistic models and sample them efficiently (Carpenter et al. 2017). Our model uses natural cubic splines with varying numbers of nodes along the stream track coordinate, ϕ_1, to describe the data in the region surrounding the Phoenix stream. To simplify the fitting process, we assume the linear density profile of the stream to be Gaussian in Φ_2, such that the stream model can

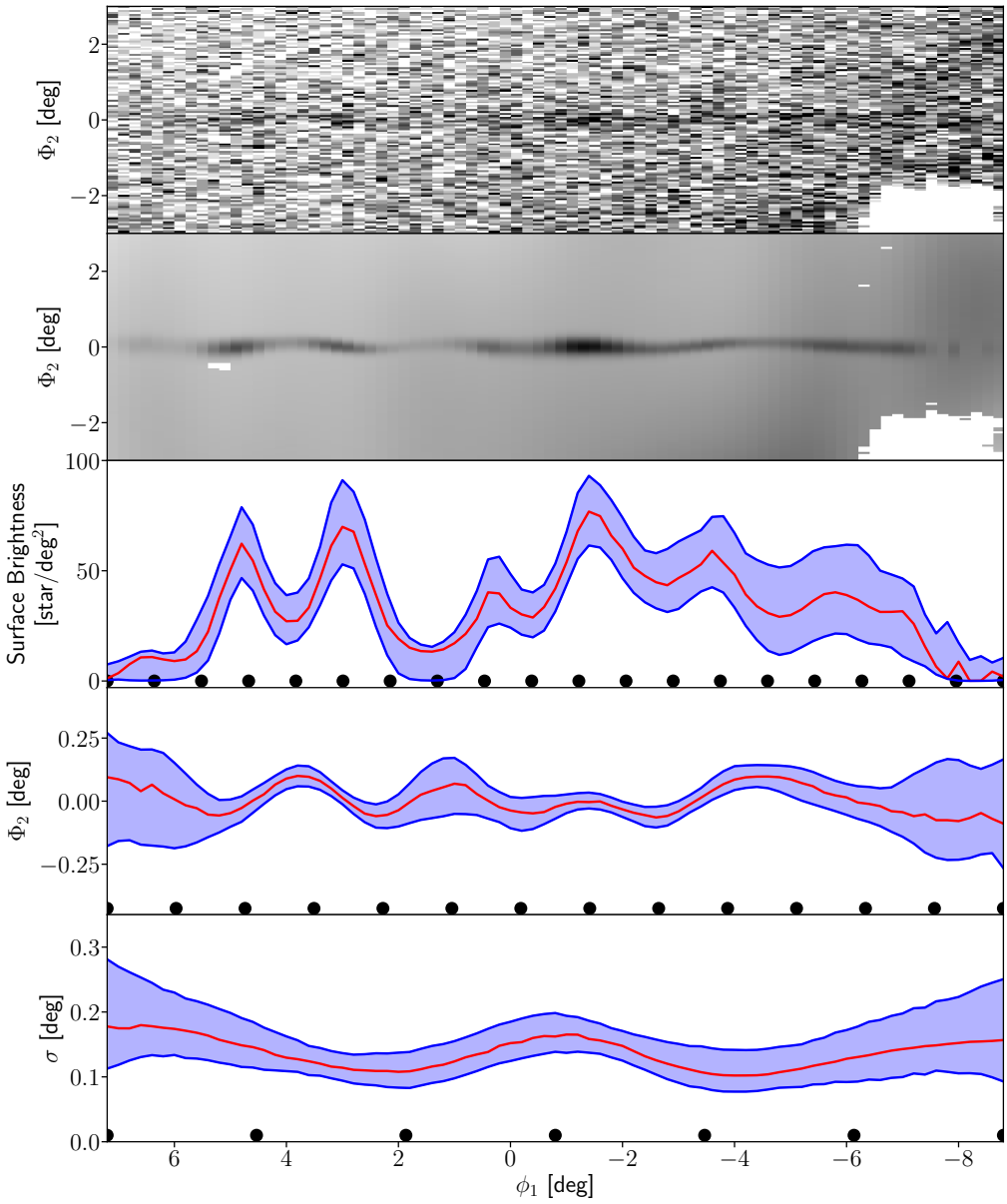

Figure 3. The results of our Phoenix stream model. *Top*: The matched filter data converted to stream coordinates and pixelized. Each pixel has a width of 0.°2 and a height of 0.°05. *Top middle*: The complete stream model computed according to Equation 1. *Middle*: The linear stream intensity, meaning the intensity at each ϕ_1 summed vertically. This does not include the background. The variation and clumpiness is immediately noticed here, with prominent peaks at $\phi_1 \approx -4$, -1.5, 3, and 5. *Bottom middle*: The stream track throughout the stream. We note the immediately apparent fluctuations. *Bottom*: The stream width along the stream. In each of the lower three panels, the red lines represent the peak of a KDE fitted to the sample outputs for each parameter. The blue shaded regions show the 1-σ uncertainty from the sample. The black dots represent the locations of the nodes used to measure each parameter.

be described by three parameters: the logarithm of the stream width, the logarithm of the stream intensity, and the stream track. We also fit the logarithm of the background density, described by a quadratic in Φ_2. Thus, the full stream and background model can be described by six parameters:

$$\rho(\phi_1, \Phi_2) = \exp[\beta(\phi_1) + \Phi_2\beta_1(\phi_1) + \Phi_2^2\beta_2(\phi_1)] + \exp[I(\phi_1)] \exp\left[-\frac{1}{2}\left(\frac{\phi_1 - \Phi_2(\phi_1)}{\exp[S(\phi_1)]}\right)^2\right]. \quad (1)$$

In this equation, β, β_1, and β_2 represent the normalization, slope, and quadratic term of the log-background, while Φ_2, S, and I represent the stream track, the stream width, and the linear stream density, respectively. The posterior distributions of the model parameters given the Phoenix data are sampled using the No-U-Turn Sampler version of the Hamilton Monte Carlo technique, which is useful for exploring high-dimensional parameter spaces efficiently (Hoffman & Gelman 2011; Neal 2012; Betancourt 2018).

The model also requires the placements of nodes for each of the six model parameters. From this, the model determines the optimal value of the given parameter at each node and constructs the cubic spline. To determine the placements of the nodes, we simplify the process by constraining them to be equidistant for each parameter. This allows us to find their positions only by specifying the number of nodes. We are then able to run Bayesian optimization to select the optimal number of nodes for each parameter using code from the GPyOpt GitHub repository .[2] We verify that our implementation of this optimization works by running it on the ATLAS stream, using the same data as in Li et al. (2020). We provide further details on this comparison in Appendix A

Applying these methods to the Phoenix stream in the DES Y6 data, we find that the stream is best described by 14, 7, 20, 15, 8, and 6 nodes for the stream track, width, linear intensity, background density, slope of the log-background, and quadratic term of the log-background, respectively. We then run 12 sampling chains for 5000 iterations, discarding the first 2000 iterations as burn-in. We ensure that each chain has converged based on a satisfactory value for the Gelman-Rubin convergence diagnostic, $\hat{R} < 1.1$ (Gelman & Rubin 1992).

The results of the model are shown in Fig. 3. We notice a number of interesting features. Most prominently, we recover a very clumpy stream, with many small scale changes in density along ϕ_1. There are four main areas of peaks in the stream intensity at $\phi_1 \approx -4$, $\phi_1 \approx -1.5$, $\phi_1 \approx 3$, and $\phi_1 \approx 5$. In addition to our observations about the stream density, we also recover small-scale variations in Φ_2 (which we also refer to as "wiggles") in the stream track. We discuss the significance of these small-scale variations in Section 5.3. In contrast to the variations in those two parameters, we find that both the stream width and background are relatively constant.

[2] http://github.com/SheffieldML/GPyOpt

4.2. *Distance Gradient*

The improved quality and depth of the DES Y6 catalog allows us to measure the distance and distance gradient of the Phoenix stream more accurately than was possible with the DES Y1 data analyzed by Balbinot et al. (2016). To measure the gradient, we create a 2D histogram model by conducting a 3-parameter search. First, we examine the raw data from DES Y6 and create isochrone selection outlines for $m - M = 14.5 - 18.0$, with one outline for each 0.01 mag, in the same fashion as described in Section 3. We then count how many stars are in each outline, providing a 1D histogram for the distance modulus of the stream. To measure the distance gradient, we then create bins in ϕ_1 and generate a 2D histogram, shown in the left panel of Fig. 4.

To create the model, we assume a linear distance gradient and a Gaussian distribution with constant width in each ϕ_1 bin. Since the stream has many clumps and gaps, we vary the peak of the Gaussian distribution in each bin accordingly. We then conduct a MCMC search to sample the posterior distributions of the distance gradient slope, the distance modulus at $\phi_1 = 0$, and the 1σ width of the Gaussian distribution that maximizes the likelihood of the model. We recover a gradient described by $m - M = (-0.001 \pm 0.002) \times \phi_1 + 16.19 \pm 0.01$. The result is shown in the central panel of Fig. 4.

This measurement of the distance gradient of the Phoenix stream is complicated by the presence of a structure overlapping the southern end of the stream. We observe this previously unidentified structure protruding into the stream path at $\phi_1 \approx -7$. This is easiest to see in Fig. 2, to the southwest of the stream. This feature is found to have a distance modulus of $m - M = 16.2$, close enough to the stream distance modulus to possibly create a distorted effect on the detected gradient. Therefore, the analysis described above excludes data at $\phi_1 < -7$. We also mask the Phoenix dwarf, located just below the stream at $\phi_1 \approx 5$ for the same purpose of non-contamination.

4.3. *Orbit Model*

We also run a dynamical model of the Phoenix stream to simulate the final debris seen in the data today. To do

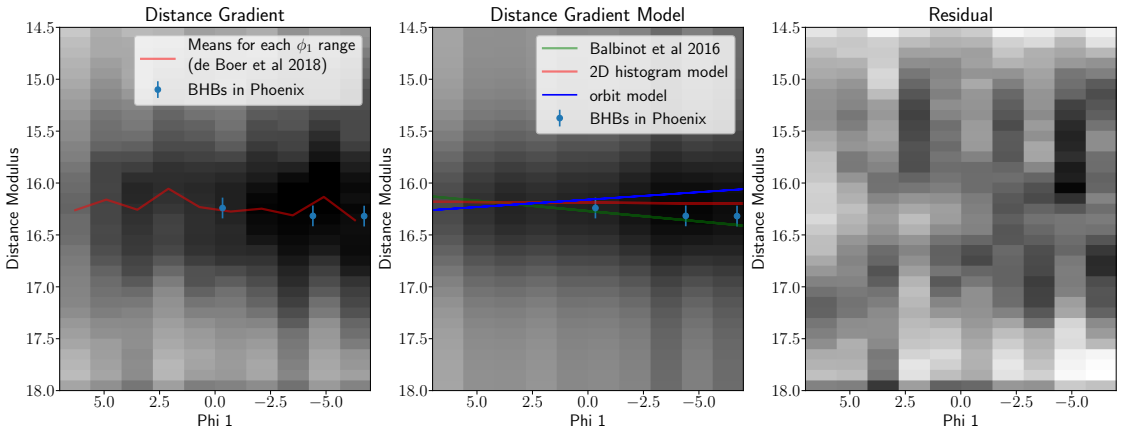

Figure 4. *Left*: A 2D histogram binning stars by ϕ_1 and distance modulus. The distance modulus binning is done by using the same matched filter selection parameters as described in Section 3 for varying $m - M$. We fit a Gaussian to the distance moduli in each ϕ_1 bin and show the means of each distribution with the red line. This is a method taken from de Boer et al. (2018) to visually track the distance gradient in a simple way. We also show three BHBs known to be members of the Phoenix stream. *Middle*: The histogram shows the 2D distance gradient model described in Section 4.2. We plot the line used to create that model in red. In green, we show the suggested gradient from Balbinot et al. (2016) and in blue we show the distance gradient suggested by the results of the orbit model described in Section 4.3. *Right*: The residual between the two 2D histograms in the left and middle panels.

this, we use the modified Lagrange Cloud Stripping technique from Gibbons et al. (2014), in which particles are stripped at the Lagrange points of the progenitor and evolved forward in the joint potential of the progenitor, Milky Way, and Large Magellanic Cloud (LMC). We model the Milky Way potential using the results of McMillan (2017), and evaluate the potential using the `galpot` code (Dehnen & Binney 1998). As in Shipp et al. (2021), we sample the MCMC chains from the McMillan (2017) fit, and use the lowest-mass realization, with $M_{\rm MW} = 8.3 \times 10^{11}\,{\rm M}_\odot$. We include an LMC, modeled as a spherical Hernquist profile (Hernquist 1990), imbedded with a Miyamoto-Nagai disk (Miyamoto & Nagai 1975). We fix the total mass of the LMC to $1.5 \times 10^{11}\,{\rm M}_\odot$, motivated by the results of Erkal et al. (2019); Shipp et al. (2021). The stream progenitor is modeled as a Plummer sphere (Plummer 1911), with a mass of $2 \times 10^4\,{\rm M}_\odot$ and a scale radius of 0.01 kpc.

We fit the dynamical model by producing mock observations of the simulated stream and calculated the likelihood via comparison to the observed stream track, radial velocity, and proper motions. We use the stream track recovered from the stream model outlined in Section 4.1. In addition, we use S^5 radial velocities and Gaia EDR3 proper motions of the member stars identified by Wan et al. (2020). We do not include distance in the likelihood calculation, but incorporate the measured distance modulus of 16.4 from Shipp et al. (2018) as a Gaussian prior with $\sigma = 0.2$. This allows for an independent prediction of the distance gradient, which we show in Fig. 4.

The best-fit model is shown in Fig. 5. In the figure, the blue points represent the simulated stream particles, and the red points are the data included in the likelihood calculation. The orbit is similar to that found by Wan et al. (2020) and Shipp et al. (2021), with $r_{\rm peri} = 12.8$ and $r_{\rm apo} = 18.3$, corresponding to an eccentricity of 0.18. In addition, we find a total energy $E_{\rm tot} = -0.19\,{\rm kpc}^2/{\rm Myr}^2$ and angular momentum perpendicular to the Galactic disk $L_{\rm z} = -1.63\,{\rm kpc}^2/{\rm Myr}$.

The orbit model recovers a distance gradient of 0.11 kpc/deg. This is in disagreement with the previously reported value from Balbinot et al. (2016), which slopes in the opposite direction. However, we should note for clarity that Balbinot et al. (2016) did not cite a distance gradient as such, but rather reported a distance modulus value for each half of the stream. We show the suggested gradient from these two values in Fig. 4. Interestingly, we observe that within the boundaries of our model and notwithstanding any additional large perturbers, a slope in the direction of that implied by Balbinot et al. (2016) is not possible.

5. DISCUSSION

5.1. *Density Variations*

Our model of the Phoenix stream demonstrates the clumpy structure of Phoenix (Fig. 3). We also show a comparison of the density fluctuations in Phoenix com-

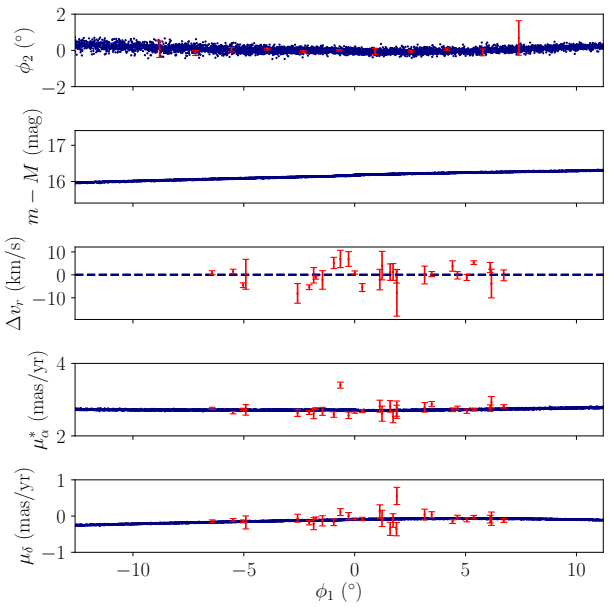

Figure 5. Dynamical model fit to the Phoenix stream data. In each panel, blue represents the best-fit model, and red represents the measurements. The first panel shows the stream track measurement presented in Section 3, where the red points indicate the best-fit ϕ_2 value and the uncertainty at each node.
Note: This dynamical model was created with a previous version of the model described in Section 4. The updated version of this model uses a slightly different matched-filter selection region. The outputs are very similar, specifically with regards to the stream track and we are therefore reasonably confident that this plot will not significantly change with the updated results.

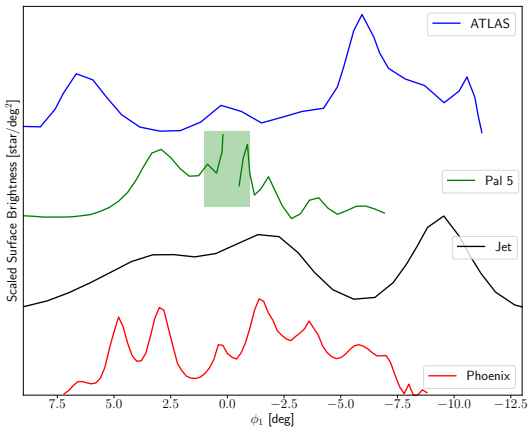

Figure 6. A comparison of four different streams modeled using the same parametric method as described in this paper. All have been scaled so that their maximum amplitudes are comparable to Phoenix's and then presented on top of one another for clarity. The shaded green area corresponds to a radius of 1 deg around the progenitor of Pal 5, which is responsible for the density fluctuations in that region. We note the smaller-scale density variations present in Phoenix relative to ATLAS and Jet and comparable to the progenitor region of Pal 5.

pared to other analyzed streams in Fig. 6. Relative to ATLAS (Li et al. 2020) or Jet (Ferguson et al. 2021), Phoenix has substantially more variation in its linear density along ϕ_1. Compared to Pal 5, it has density variations on slightly larger scales to the ones near Pal 5's progenitor. Pal 5 also has other density fluctuations on small scales farther from its progenitor, but those are smaller in magnitude compared to Phoenix's. We therefore conclude that Phoenix is the clumpiest stream modeled in this way.

We also observe a few other noticeable traits about Phoenix. We find that the southern part of the stream ($\phi_1 < 0$) is more dense than the northern section. We detect peaks at $\phi_1 \approx -4$, -1.5, 3, 5 and underdense regions (gaps) at $\phi_1 \approx -5$, -3, 1, 4.

Interestingly, if we group these four peaks into two groups of two by location ($\phi_1 \approx 3, 5$ and $\phi_1 \approx -4, -1.5$), they have a number of attributes worth comparing. In each set, there is approximately 2 degrees between the peaks. However, while the two in the northern half of the stream ($\phi_1 \approx 3$ and 5) attain almost the same maximum surface brightness, the two overdensities in the southern part of the stream reach different maxima. Furthermore, the gap between the peaks in the northern half of the stream is much deeper, while in the southern half, the underdensity is less pronounced. Comparing these two areas could help us understand the mechanism behind the creation of each feature. For example, similar attributes, such as the scale of the separation between peaks could suggest that the two were formed by the same type and size of perturber.

In addition to the gaps associated between each set of peaks, there is also a notable and prominent gap in the interval $\phi_1 \approx (0, 2)$. In this region, the stream density descends to its lowest point and remains there for an extended stretch of a couple degrees, in contrast to the rest of the stream density, which changes on degree scales. This difference might suggest a different origin for the gap; one which would cause a deeper and more extensive impact. It is likely that this feature was caused by a more massive perturber, capable of generating a large disturbance in the stream.

These peaks and gaps can form in a variety of different ways which we explore in this section. Figuring out the causes of each inhomogeneity can help us determine

the ways in which various structures, particularly dark matter subhalos, in the Milky Way interact with stellar streams.

5.2. *Distance Gradient*

Our best-fit distance gradient, $m - M = (-0.001 \pm 0.002) \times \phi_1 + 16.19 \pm 0.01$, does not quite agree with that suggested by Balbinot et al. (2016). It finds more or less no gradient along the stream. Furthermore, the results of our orbit modeling in Section 4.3 disfavor a distance gradient in the direction suggested by Balbinot et al. (2016). In fact, it would be impossible for the stream to have a gradient in that direction without an additional large perturber not used in the orbit model. From this information, we find it likely that flat result from our distance gradient model is an improved estimate for the true gradient of the Phoenix stream. This result would suggest almost no change in distance modulus along the stream, with a maximum difference of about 0.1 mags between the northern and southern ends.

5.3. *Stream Track Variations*

Small scale variations in stream tracks have not been studied as extensively as stream density changes so far. The results we present from our stream model gives the opportunity to consider what might cause such "wiggles" as seen in the last panel of Fig. 3. The first thing to determine is whether these fluctuations are real in Phoenix, or if they are caused by the model.

Tidal debris precesses and nutates in an aspherical potential because angular momentum is no longer conserved (e.g. (Ibata et al. 2001; Helmi 2004; Johnston et al. 2005; Belokurov et al. 2014; Erkal et al. 2016)). In such potentials, the stream track is expected to deviate gradually and smoothly from the great circle (Erkal et al. 2017). However, such models do not predict small scale features in the stream track in a representative galaxy such as the Milky Way (Erkal et al. 2017). We note that the while it does wiggle, the amplitude of the fluctuations remains less than the reported stream width. This could indicate that the model had trouble locating the exact center of the density distribution at each ϕ_1 and therefore created what would be artificial wiggles for a straight line stream track (de Boer et al. 2018). Another possibility is that the density perturbations artificially caused the the model to see stream track variations as well. These do not seem particularly likely since the uncertainties on both the width and the track are rather small and the variations in the stream track generally do not line up with the overdense regions.

Therefore, although we do not rule out completely the idea that these wiggles are artificially created by the model, we believe it more likely that they are real features of the Phoenix stream. We quantify this estimate by comparing the log-likelihood of the model with the log-likelihood generated when requiring a flat track. This yields a significance of 1.0σ for the stream wiggles.

One potential cause of the stream track variations is interaction with perturbers. These would likely be the same interactions that caused the density fluctuations discussed in the Section 5.1. Given the clumpy nature of the stream overall, it is likely that Phoenix has come into contact with a number of perturbers that could have an effect on both the density and the track. One outcome of these interactions could be that stream members developed line-of-sight velocities. The perturbations would have affected certain areas more than others, disturbing the motion and velocities of some stars. This would pull them away from the great circle track and manifest as wiggles, explaining the deviations in the stream track (Koposov et al. 2019). Lastly, we note the possibility of a perturbation caused by the progenitor. The progenitor is known to cause stream track deviations in other streams such as Palomar 5 (Erkal et al. 2017; Bonaca et al. 2020). Recently, Li et al. (2020) showed that wiggles on the scale of tenths of degrees could be caused by a progenitor. That leaves open the possibility of that explanation for one of these wiggles.

5.4. *Density Variation Interpretations*

5.4.1. *Stream Formation*

Density variations can be introduced in a variety of ways, one of which is as part of stream formation. As stars escape from their progenitor masses to create the tidal features, their epicycle motion sometimes slows when they get farther from the star cluster. This tends to happen at a similar location for many stars because of the similarity in initial positions and velocities, leading to a clump (Küpper et al. 2008). In theory this would create a single overdensity at some distance from the progenitor. This distance depends on the stream's orbit, the progenitor mass, and the strength of the tidal field (Küpper et al. 2010).

Another intriguing idea is that density variations could be introduced if the Phoenix stream originated from a globular cluster accreted within a parent satellite galaxy. Due to its thin width and the fact that it is dynamically cold, Phoenix's progenitor is likely to have been a globular cluster. The low metallicity of the Phoenix stream may suggest that it was formed and accreted as part of a low-mass galaxy (Balbinot et al. 2016). Malhan et al. (2020) suggested that streams formed from globular clusters within accreting satellite galaxies may be perturbed by the parent satellite. Be-

cause the stream and its parent satellite are on similar orbits, there is a longer time where the two structures are in close proximity to one another and the gravity from the parent subhalo can affect the uniformity of the stream. In addition to causing gaps in the stream, a similar process can also lead to narrow spikes in the stream density, similar to what we observe from the model results. This happens because as the subhalo orbits the Milky Way, variations in its mass loss rate cause it to periodically deposit increased globular cluster stellar debris (Malhan et al. 2020).

Malhan et al. (2020) also demonstrated that the morphology of globular cluster streams that originated in accreting satellites can be sensitive to the density profile of the dark matter subhalo that hosted the satellite. Streams that form from globular clusters accreted in cuspy dark matter subhalos tend to be slightly wider, although not as wide as those with dwarf galaxy progenitors, and more often contain a cocoon component, meaning a wider distribution of part of the stream. They also tend to be more disrupted, with additional density variations caused in part by the lower tidal radius of those globular clusters.

5.4.2. *Milky Way Structure*

Baryonic structures in the Milky Way can also introduce density variations in stellar streams. Previous work has modelled the effect of baryonic disrupters such as the Milky Way bar Pearson et al. (2017) or spiral arms Banik & Bovy (2019). The effect of the bar can be understood by noting that since each stream is on an orbit, different stars along the stream reach pericenter at different times. If the bar is rotating, then these stars will experience unequal torques, causing a redistribution of energy along the stream (Hattori et al. 2016). This in turn would lead to a different growth rates along the stream, potentially resulting in ever-widening gaps in the stream intensity (Pearson et al. 2017). Spiral arms were also shown to have an effect on stream density. They are more likely to induce degree-scale fluctuations with less severe variations in the intensity of each clump (Banik & Bovy 2019). These are the kind of variations that are apparent in Phoenix from our model.

Models of these perturbers have been made to examine their possible effects on other streams (Banik & Bovy 2019; Pearson et al. 2017; Erkal et al. 2017). This allowed them to trace certain variations to specific perturbers, furthering the understanding of how different structures interact in the Milky Way. In this work, we do not present any such models or simulations but rather seek to present the different types of disturbers that could have had an effect on the Phoenix stream. We leave the modelling work to narrow down those perturbers responsible for specific variations to a future study.

5.4.3. *Halo Perturbers*

Some of the possible disrupters are known halo perturbers in the Milky Way. These include the Large and Small Magellanic Clouds (LMC and SMC), other known satellites such as Sagittarius, globular clusters, and giant molecular clouds (GMCs). Each of these can have an influence on any stream that crosses them or comes near. The LMC, for instance, could create a reflex motion in the Milky Way and has been shown to affect the orbit of the Sagittarius stream (Gómez et al. 2015). Sagittarius itself passes within $\sim$ 7 kpc of Phoenix, meaning it could have its own gravitational effect on certain parts of the stream. Globular clusters, although smaller, can also exert gravitational influence on certain parts of streams. In fact, because of their smaller size, they are more likely to induce smaller-scale variations of the kind seen in Phoenix than larger objects like the LMC or SMC. Lastly, GMCs have been shown to have important effects on streams (Amorisco et al. 2016). N-body simulations have shown that GMC disks can cause gaps and clumps in streams evolving around them. This analysis was performed on Pal 5 and GD-1 by Amorisco et al. (2016), who concluded that these GMCs could cause disturbances in cold thin streams similar to those created by dark matter subhalo flybys.

Such dark matter subhalos in the Milky Way are among the unknown possible perturbances to the density of the stream. When simulating the effect of a subhalo on idealized streams it is clear that such structures can cause both large and small variations in the stream density (Ibata et al. 2002; Johnston et al. 2002). Full dark matter subhalos can create fluctuations of $2 - 6^{\circ}$ along ϕ_1 while lower mass subhalos can create smaller scale discrepancies (Carlberg 2020).

Streams can be used to gain greater knowledge about dark matter subhalos. It is possible to reliably determine a subhalo's mass and size based on the gap it creates in a stellar stream (Erkal & Belokurov 2015b). There has also been work done to track the location of dark matter subhalos based on the density variations they cause in streams (Bonaca et al. 2019). Clearly, analyzing stellar stream densities and the way they vary can give great information about dark matter subhalos that we are still seeking to understand, and looking at the fluctuations in Phoenix could be a way to do that.

6. CONCLUSIONS

In this paper, we have used the new DES Year 6 data to conduct a deeper analysis of the Phoenix stellar

stream. We apply a non-parametric stream model using natural splines to determine stream properties such as the stream track, width, and linear density. Our model makes few *a priori* assumptions about the structure of the Phoenix stream and therefore the model complexity comes directly from the data. This model prefers a clumpy stream density distribution throughout the entire length of the stream. These clumps and gaps vary in angular size as well as their maximum and minimum linear intensities. We also observe wiggles in the stream track, which have a 1σ significance. Such small scale wiggles would be a rare occurrence for stellar streams in aspherical potentials such as in the Milky Way (Erkal et al. 2017).

We also measure the distance and distance gradient of the Phoenix stream and find that it has a very small gradient, -0.01 ± 0.02 kpc/deg. Our measured distance gradient is in relative good agreement with an orbital model built on the track and mean distance of the Phoenix stream and the proper motion and radial velocities of stream members.

We consider the potential causes of these variations in both density and track. In particular, we discuss the stream's interaction with both baryonic perturbers and dark matter subhalos as possibly leaving the clumps, gaps, and wiggles we observe. Because of the relatively large number of clumps and fluctuations relative to other streams, we believe it likely that disturbances from the parent satellite may have played a large role in the stream structure today.

The function of this paper is to lay the groundwork for future analysis on the formation and evolution of the Phoenix stellar stream. We hope that by providing a more detailed analysis of the stream using deeper data, our results will enable others to run more advanced models to simulate the clumps and wiggles found here. Such work would then go a long way towards helping us understand the interactions of various structures within our own Milky Way and form the groundwork for similar analyses and models on other streams.

7. ACKNOWLEDGMENTS

I would like to thank Alex Drlica-Wagner for giving me the opportunity to conduct this research and providing access to the DES data. I am grateful for his continued guidance and assistance to tackle the trickier aspects of this analysis. I would also like to thank Nora Shipp and Peter Ferguson for helping with some of the analysis along with their input during our weekly meetings. Lastly, thank you to my family, whose support throughout this research has been invaluable.

Funding for the DES Projects has been provided by the U.S. Department of Energy, the U.S. National Science Foundation, the Ministry of Science and Education of Spain, the Science and Technology Facilities Council of the United Kingdom, the Higher Education Funding Council for England, the National Center for Supercomputing Applications at the University of Illinois at Urbana-Champaign, the Kavli Institute of Cosmological Physics at the University of Chicago, the Center for Cosmology and Astro-Particle Physics at the Ohio State University, the Mitchell Institute for Fundamental Physics and Astronomy at Texas A&M University, Financiadora de Estudos e Projetos, Fundação Carlos Chagas Filho de Amparo à Pesquisa do Estado do Rio de Janeiro, Conselho Nacional de Desenvolvimento Científico e Tecnológico and the Ministério da Ciência, Tecnologia e Inovação, the Deutsche Forschungsgemeinschaft and the Collaborating Institutions in the Dark Energy Survey.

The Collaborating Institutions are Argonne National Laboratory, the University of California at Santa Cruz, the University of Cambridge, Centro de Investigaciones Energéticas, Medioambientales y Tecnológicas-Madrid, the University of Chicago, University College London, the DES-Brazil Consortium, the University of Edinburgh, the Eidgenössische Technische Hochschule (ETH) Zürich, Fermi National Accelerator Laboratory, the University of Illinois at Urbana-Champaign, the Institut de Ciències de l'Espai (IEEC/CSIC), the Institut de Física d'Altes Energies, Lawrence Berkeley National Laboratory, the Ludwig-Maximilians Universität München and the associated Excellence Cluster Universe, the University of Michigan, the National Optical Astronomy Observatory, the University of Nottingham, The Ohio State University, the University of Pennsylvania, the University of Portsmouth, SLAC National Accelerator Laboratory, Stanford University, the University of Sussex, Texas A&M University, and the OzDES Membership Consortium.

Based in part on observations at Cerro Tololo Inter-American Observatory, National Optical Astronomy Observatory, which is operated by the Association of Universities for Research in Astronomy (AURA) under a cooperative agreement with the National Science Foundation.

The DES data management system is supported by the National Science Foundation under Grant Numbers AST-1138766 and AST-1536171. The DES participants from Spanish institutions are partially supported by MINECO under grants AYA2015-71825, ESP2015-66861, FPA2015-68048, SEV-2016-0588, SEV-2016-0597, and MDM-2015-0509, some of which include

ERDF funds from the European Union. IFAE is partially funded by the CERCA program of the Generalitat de Catalunya. Research leading to these results has received funding from the European Research Council under the European Union's Seventh Framework Program (FP7/2007-2013) including ERC grant agreements 240672, 291329, and 306478. We acknowledge support from the Australian Research Council Centre of Excellence for All-sky Astrophysics (CAASTRO), through project number CE110001020, and the Brazilian Instituto Nacional de Ciência e Tecnologia (INCT) e-Universe (CNPq grant 465376/2014-2).

This manuscript has been authored by Fermi Research Alliance, LLC under Contract No. DE-AC02-07CH11359 with the U.S. Department of Energy, Office of Science, Office of High Energy Physics. The United States Government retains and the publisher, by accepting the article for publication, acknowledges that the United States Government retains a non-exclusive, paid-up, irrevocable, world-wide license to publish or reproduce the published form of this manuscript, or allow others to do so, for United States Government purposes.

This work has made use of data from the European Space Agency (ESA) mission *Gaia* (https://www.cosmos.esa.int/gaia), processed by the *Gaia* Data Processing and Analysis Consortium (DPAC, https://www.cosmos.esa.int/web/gaia/dpac/consortium). Funding for the DPAC has been provided by national institutions, in particular the institutions participating in the *Gaia* Multilateral Agreement.

Based on data acquired at the Anglo-Australian Telescope. We acknowledge the traditional owners of the land on which the AAT stands, the Gamilaroi people, and pay our respects to elders past and present.

REFERENCES

Abbott, T. M. C., Adamow, M., Aguena, M., et al. 2021, The Dark Energy Survey Data Release 2. https://arxiv.org/abs/2101.05765

Abbott, T. M. C., Adamow, M., Aguena, M., et al. 2021, arXiv e-prints, arXiv:2101.05765. https://arxiv.org/abs/2101.05765

Amorisco, N. C., Gómez, F. A., Vegetti, S., & White, S. D. M. 2016, Monthly Notices of the Royal Astronomical Society: Letters, 463, L17–L21, doi: 10.1093/mnrasl/slw148

Balbinot, E., Yanny, B., Li, T. S., et al. 2016, The Astrophysical Journal, 820, 58, doi: 10.3847/0004-637x/820/1/58

Banik, N., & Bovy, J. 2019, Monthly Notices of the Royal Astronomical Society, 484, 2009–2020, doi: 10.1093/mnras/stz142

Bechtol, K., Drlica-Wagner, A., Balbinot, E., et al. 2015, The Astrophysical Journal, 807, 50, doi: 10.1088/0004-637x/807/1/50

Becker, M. R. 2015, arXiv e-prints, arXiv:1507.03605. https://arxiv.org/abs/1507.03605

Belokurov, V., Zucker, D. B., Evans, N. W., et al. 2006, ApJL, 642, L137, doi: 10.1086/504797

Belokurov, V., Koposov, S. E., Evans, N. W., et al. 2014, MNRAS, 437, 116, doi: 10.1093/mnras/stt1862

Betancourt, M. 2018, A Conceptual Introduction to Hamiltonian Monte Carlo. https://arxiv.org/abs/1701.02434

Bonaca, A., Hogg, D. W., Price-Whelan, A. M., & Conroy, C. 2019, The Astrophysical Journal, 880, 38, doi: 10.3847/1538-4357/ab2873

Bonaca, A., Pearson, S., Price-Whelan, A. M., et al. 2020, The Astrophysical Journal, 889, 70, doi: 10.3847/1538-4357/ab5afe

Brown, A. G. A., Vallenari, A., Prusti, T., et al. 2021, Astronomy Astrophysics, 649, A1, doi: 10.1051/0004-6361/202039657

Burke, D. L., Rykoff, E. S., Allam, S., et al. 2017, The Astronomical Journal, 155, 41, doi: 10.3847/1538-3881/aa9f22

Carlberg, R. G. 2020, ApJ, 889, 107, doi: 10.3847/1538-4357/ab61f0

Carpenter, B., Gelman, A., Hoffman, M., et al. 2017, Journal of Statistical Software, Articles, 76, 1, doi: 10.18637/jss.v076.i01

Conroy, C., & Wechsler, R. H. 2009, ApJ, 696, 620, doi: 10.1088/0004-637X/696/1/620

de Boer, T. J. L., Belokurov, V., Koposov, S. E., et al. 2018, Monthly Notices of the Royal Astronomical Society, 477, 1893–1902, doi: 10.1093/mnras/sty677

Dehnen, W., & Binney, J. 1998, MNRAS, 294, 429, doi: 10.1046/j.1365-8711.1998.01282.x

DES Collaboration. 2005, ArXiv Astrophysics e-prints

—. 2016, MNRAS, 460, 1270, doi: 10.1093/mnras/stw641

Diemand, J., Moore, B., & Stadel, J. 2005, Nature, 433, 389, doi: 10.1038/nature03270

Dotter, A., Chaboyer, B., Jevremović, D., et al. 2008, ApJS, 178, 89, doi: 10.1086/589654

Drlica-Wagner, A., Bechtol, K., Rykoff, E. S., et al. 2015, The Astrophysical Journal, 813, 109, doi: 10.1088/0004-637x/813/2/109

Drlica-Wagner, A., Sevilla-Noarbe, I., Rykoff, E. S., et al. 2018, ApJS, 235, 33, doi: 10.3847/1538-4365/aab4f5

Erkal, D., & Belokurov, V. 2015a, Monthly Notices of the Royal Astronomical Society, 450, 1136–1149, doi: 10.1093/mnras/stv655

—. 2015b, Monthly Notices of the Royal Astronomical Society, 454, 3542–3558, doi: 10.1093/mnras/stv2122

Erkal, D., Koposov, S. E., & Belokurov, V. 2017, Monthly Notices of the Royal Astronomical Society, 470, 60–84, doi: 10.1093/mnras/stx1208

Erkal, D., Sanders, J. L., & Belokurov, V. 2016, MNRAS, 461, 1590, doi: 10.1093/mnras/stw1400

Erkal, D., Belokurov, V., Laporte, C. F. P., et al. 2019, MNRAS, 487, 2685, doi: 10.1093/mnras/stz1371

Ferguson, P., Shipp, N., Drlica-Wagner, A., et al. 2021, arXiv e-prints, arXiv:2104.11755. https://arxiv.org/abs/2104.11755

Flaugher, B., Diehl, H. T., Honscheid, K., et al. 2015, AJ, 150, 150, doi: 10.1088/0004-6256/150/5/150

Gaia Collaboration, Prusti, T., de Bruijne, J. H. J., et al. 2016, A&A, 595, A1, doi: 10.1051/0004-6361/201629272

Gelman, A., & Rubin, D. B. 1992, Statist. Sci., 7, 457, doi: 10.1214/ss/1177011136

Gibbons, S. L. J., Belokurov, V., & Evans, N. W. 2014, MNRAS, 445, 3788, doi: 10.1093/mnras/stu1986

Gómez, F. A., Besla, G., Carpintero, D. D., et al. 2015, ApJ, 802, 128, doi: 10.1088/0004-637X/802/2/128

Grillmair, C. J., & Carlin, J. L. 2016, Astrophysics and Space Science Library, 87–112, doi: 10.1007/978-3-319-19336-6_4

Guo, Q., White, S., Angulo, R. E., et al. 2013, MNRAS, 428, 1351, doi: 10.1093/mnras/sts115

Hattori, K., Erkal, D., & Sanders, J. L. 2016, Monthly Notices of the Royal Astronomical Society, 460, 497–512, doi: 10.1093/mnras/stw1006

Helmi, A. 2004, Monthly Notices of the Royal Astronomical Society, 351, 643–648, doi: 10.1111/j.1365-2966.2004.07812.x

Helmi, A., & White, S. D. M. 1999, Monthly Notices of the Royal Astronomical Society, 307, 495–517, doi: 10.1046/j.1365-8711.1999.02616.x

Hernquist, L. 1990, ApJ, 356, 359, doi: 10.1086/168845

Hoffman, M. D., & Gelman, A. 2011, The No-U-Turn Sampler: Adaptively Setting Path Lengths in Hamiltonian Monte Carlo. https://arxiv.org/abs/1111.4246

Ibata, R., Lewis, G. F., Irwin, M., Totten, E., & Quinn, T. 2001, The Astrophysical Journal, 551, 294–311, doi: 10.1086/320060

Ibata, R. A., Lewis, G. F., Irwin, M. J., & Quinn, T. 2002, Monthly Notices of the Royal Astronomical Society, 332, 915–920, doi: 10.1046/j.1365-8711.2002.05358.x

Johnston, K. V. 1998, The Astrophysical Journal, 495, 297–308, doi: 10.1086/305273

Johnston, K. V., Law, D. R., & Majewski, S. R. 2005, The Astrophysical Journal, 619, 800–806, doi: 10.1086/426777

Johnston, K. V., Spergel, D. N., & Haydn, C. 2002, The Astrophysical Journal, 570, 656–664, doi: 10.1086/339791

Koposov, S. E., Belokurov, V., Li, T. S., et al. 2019, Monthly Notices of the Royal Astronomical Society, 485, 4726–4742, doi: 10.1093/mnras/stz457

Küpper, A. H. W., Kroupa, P., Baumgardt, H., & Heggie, D. C. 2010, MNRAS, 401, 105, doi: 10.1111/j.1365-2966.2009.15690.x

Küpper, A. H. W., MacLeod, A., & Heggie, D. C. 2008, MNRAS, 387, 1248, doi: 10.1111/j.1365-2966.2008.13323.x

Li, T. S., Koposov, S. E., Zucker, D. B., et al. 2019, MNRAS, 490, 3508, doi: 10.1093/mnras/stz2731

Li, T. S., Koposov, S. E., Erkal, D., et al. 2020, Broken into Pieces: ATLAS and Aliqa Uma as One Single Stream. https://arxiv.org/abs/2006.10763

Malhan, K., Valluri, M., & Freese, K. 2020, Probing the nature of dark matter with accreted globular cluster streams. https://arxiv.org/abs/2005.12919

McMillan, P. J. 2017, MNRAS, 465, 76, doi: 10.1093/mnras/stw2759

Miyamoto, M., & Nagai, R. 1975, Publications of the Astronomical Society of Japan, 27, 533

Morganson, E., Gruendl, R. A., Menanteau, F., et al. 2018, Publications of the Astronomical Society of the Pacific, 130, 074501, doi: 10.1088/1538-3873/aab4ef

Neal, R. M. 2012, MCMC using Hamiltonian dynamics. https://arxiv.org/abs/1206.1901

Odenkirchen, M., Grebel, E. K., Dehnen, W., Rix, H.-W., & Cudworth, K. M. 2002, The Astronomical Journal, 124, 1497–1510, doi: 10.1086/342287

Odenkirchen, M., Grebel, E. K., Rockosi, C. M., et al. 2001, The Astrophysical Journal, 548, L165–L169, doi: 10.1086/319095

Odenkirchen, M., Grebel, E. K., Dehnen, W., et al. 2003, The Astronomical Journal, 126, 2385–2407, doi: 10.1086/378601

Pearson, S., Price-Whelan, A. M., & Johnston, K. V. 2017, Nature Astronomy, 1, 633, doi: 10.1038/s41550-017-0220-3

Plummer, H. C. 1911, MNRAS, 71, 460, doi: 10.1093/mnras/71.5.460

Rockosi, C. M., Odenkirchen, M., Grebel, E. K., et al. 2002, The Astronomical Journal, 124, 349, doi: 10.1086/340957

Sevilla-Noarbe, I., Bechtol, K., Kind, M. C., et al. 2020, Dark Energy Survey Year 3 Results: Photometric Data Set for Cosmology. https://arxiv.org/abs/2011.03407

Shipp, N., Erkal, D., Drlica-Wagner, A., et al. 2021, in prep.

Shipp, N., Drlica-Wagner, A., Balbinot, E., et al. 2018, The Astrophysical Journal, 862, 114, doi: 10.3847/1538-4357/aacdab

Wan, Z., Lewis, G. F., Li, T. S., et al. 2020, Nature, 583, 768–770, doi: 10.1038/s41586-020-2483-6

Wang, J., Bose, S., Frenk, C. S., et al. 2020, Nature, 585, 39, doi: 10.1038/s41586-020-2642-9

Wechsler, R. H., & Tinker, J. L. 2018, ARA&A, 56, 435, doi: 10.1146/annurev-astro-081817-051756

APPENDIX

A. VERIFYING THE MODEL WITH ATLAS

In order to verify the proper functioning of our slightly updated model from versions used for previous streams, we attempt to replicate the results from Li et al. (2020) for the ATLAS stream. We use the same data three-year DES data used in that paper and run the analysis we intend to run on Phoenix. We first determine the optimal number of nodes for each of the six parameters described in Section 4, before running a maximum log-likelihood optimization for the best fit curves of each parameter. Due to complexity of the six parameters, the limited run time of the node optimization, and the different cross-validation subsets used in our analysis versus the published one, we do not recover the exact same number of nodes for each parameter. However, we find excellent agreement (green and blue curves in Fig. A.1) in the curves for the intensity, track, and width with the published results from Li et al. (2020). The ability to replicate previous results builds confidence in our ability to characterize Phoenix in a manner similar to that previously applied to other streams.

Before applying the model to Phoenix, we also want to verify that switching to the new and deeper DES Y6 dataset does not have any artificial impact on the stream features by running the same optimization on the ATLAS stream but with the new data. We again recover slightly different numbers of nodes, but an outcome that agrees with the previously published results and our re-analysis of the Y3 data as seen in Fig. A.1.

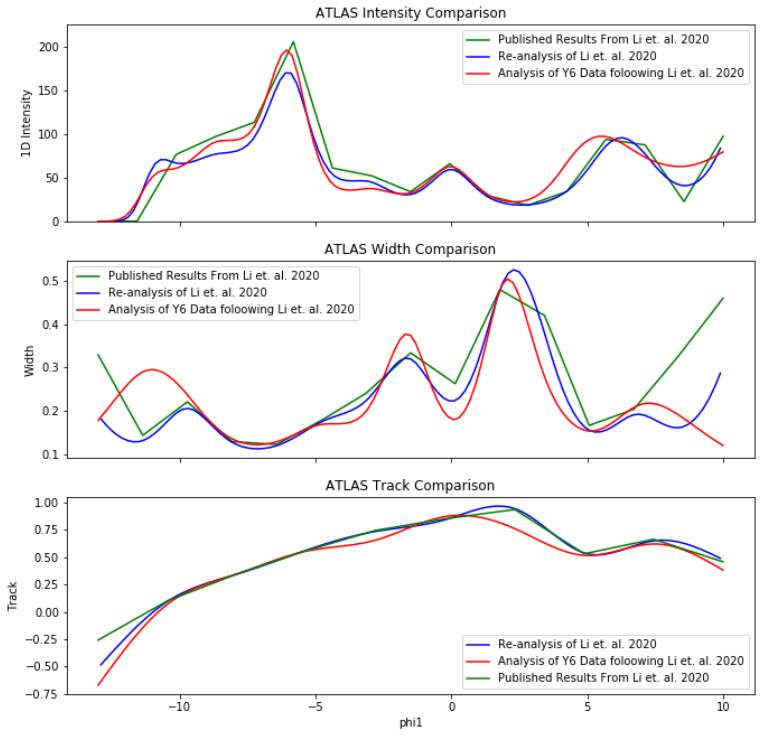

Figure A.1. We test that our model works properly by replicating the results from Li et al. (2020). We show a comparison between the 1D intensities, widths, and tracks in the three panels. The green curve shows the published results from Li et al. (2020). The blue curve shows our re-analysis using the same Y3 data as that paper used. The red curve shows an analysis using the deeper Y6 data. We clearly see a good agreement for all three curves. This gives us confidence that our model works properly and that the new data does not have any artificial impacts on the stream features.